Revisiting the contemporary sea-level budget on global and regional scales

Roelof Rietbroek[a,1], Sandra-Esther Brunnabend[a,b], Jürgen Kusche[a], Jens Schröter[b], and Christoph Dahle[c]

[a]Institute of Geodesy and Geoinformation, University of Bonn, D-53115 Bonn, Germany; [b]Alfred Wegener Institute for Polar and Marine Research, D-27570 Bremerhaven, Germany; and [c]GFZ German Research Centre for Geosciences, D-14473 Potsdam, Germany

Edited by Anny Cazenave, Centre National d'Etudes Spatiales, Toulouse, France, and approved November 30, 2015 (received for review September 29, 2015)

Dividing the sea-level budget into contributions from ice sheets and glaciers, the water cycle, steric expansion, and crustal movement is challenging, especially on regional scales. Here, Gravity Recovery And Climate Experiment (GRACE) gravity observations and sea-level anomalies from altimetry are used in a joint inversion, ensuring a consistent decomposition of the global and regional sea-level rise budget. Over the years 2002–2014, we find a global mean steric trend of 1.38 ± 0.16 mm/y, compared with a total trend of 2.74 ± 0.58 mm/y. This is significantly larger than steric trends derived from in situ temperature/salinity profiles and models which range from 0.66 ± 0.2 to 0.94 ± 0.1 mm/y. Mass contributions from ice sheets and glaciers (1.37 ± 0.09 mm/y, accelerating with 0.03 ± 0.02 mm/y^2) are offset by a negative hydrological component (−0.29 ± 0.26 mm/y). The combined mass rate (1.08 ± 0.3 mm/y) is smaller than previous GRACE estimates (up to 2 mm/y), but it is consistent with the sum of individual contributions (ice sheets, glaciers, and hydrology) found in literature. The altimetric sea-level budget is closed by coestimating a remaining component of 0.22 ± 0.26 mm/y. Well above average sea-level rise is found regionally near the Philippines (14.7 ± 4.39 mm/y) and Indonesia (8.3 ± 4.7 mm/y) which is dominated by steric components (11.2 ± 3.58 mm/y and 6.4 ± 3.18 mm/y, respectively). In contrast, in the central and Eastern part of the Pacific, negative steric trends (down to −2.8 ± 1.53 mm/y) are detected. Significant regional components are found, up to 5.3 ± 2.6 mm/y in the northwest Atlantic, which are likely due to ocean bottom pressure variations.

sea level | budget | steric | GRACE | altimetry

Global sea-level rise has been identified as one of the major threats associated with global climate change (1, 2). However, from the perspective of assessment- and decision-making, regional estimates of sea-level rise are even more important to formulate meaningful adaptation plans on a national or international level. Besides the magnitude of the total sea-level rise itself, identifying dominant drivers, and their corresponding uncertainties, may also prove beneficial for projection studies.

Historical records from tide gauges indicate a sea-level rate of about 1.7 mm/y over the period 1900–2009, where it must be noted that tide gauges indicate an acceleration (0.009–0.017 mm/y^2) over the last century (3–5). Besides the steric expansion of sea water due to temperature changes, the ongoing melting and ablation of ice sheets in Greenland and Antarctica and other land glaciers cause the sea level to rise. Hydrological mass variability on land and reservoir construction have been found to cause a negative trend (6–9). Furthermore, meltwater, precipitation, or evaporation result in regional salinity changes, leaving steric signatures in sea level once the barotropic component has been compensated (10). For an observer at the coast, crustal movement, caused by glacial isostatic adjustment (GIA), tectonics, or local subsidence may also significantly affect the relative sea level. Finally, sea level may be altered regionally by long-term changes in wind stress, atmospheric pressure, and changes in heat and freshwater fluxes at the ocean surface and boundaries (e.g., ref. 11).

It is well known that sea level does not rise uniformly across the ocean basins, but exhibits regional variations (12). Global mean sea level provides an excellent metric to monitor global change, and ample studies exist which attempt to close the global mean sea-level budget in terms of the different contributions (12–15). Unfortunately, the components of the sea-level budget still exhibit significant differences across studies depending on the chosen corrections, datasets, methods, and time periods (16, 17).

Understanding sea-level rise requires a well-established monitoring network, preferably covering long timespans. Besides important historic measurements from reprocessed tide gauge measurements (18), spaceborn techniques have become increasingly important over the last decades. Satellite radar altimetry enabled monitoring of geometric sea level with unprecedented coverage, and more recently, satellite gravimetry from the Gravity Recovery And Climate Experiment (GRACE) provided invaluable information on mass contributions to sea level. Because altimetry and gravimetry measure different contributions of sea-level change, i.e., total versus mass-driven, combining them allows one to resolve for volumetric (steric) sea-level changes.

Independently, steric sea level can also be resolved by integrating volumetric anomalies over a water column, from measured temperature and salinity changes. Hydrographic profiles of temperature and salinity can be derived from expendable bathythermography (XBT), conductivity/depth/temperature and, in more recent times, from Argo floats (e.g., ref. 19).

Here, we decompose global and regional sea level into different components (steric, glaciers and ice sheets, hydrology, GIA) by combining sea-level anomalies from Jason-1/2 and

Significance

Understanding sea-level change is of paramount importance because it reflects climate-related factors, such as the ocean heat budget, mass changes in the cryosphere, and natural ocean/atmosphere variations. Furthermore, sea-level rise directly affects coastal areas, which has ramifications for its population and economy. From a novel combination of Gravity Recovery And Climate Experiment and radar altimetry data we find over the last 12 y: (*i*) a larger global steric sea-level rise as previously reported, (*ii*) a mass contribution to global sea level consistent with mass loss estimates from the world's ice sheets, glaciers, and hydrological sources, and (*iii*) regionally resolved sea-level budget components which differ significantly from that of the global sea-level budget.

Author contributions: R.R. designed research; R.R. and S.-E.B. performed research; R.R., S.-E.B., and C.D. analyzed data; and R.R., J.K., and J.S. wrote the paper.

The authors declare no conflict of interest.

This article is a PNAS Direct Submission.

Data deposition: The data reported in this paper have been deposited in the PANGAEA database, www.pangaea.de (doi: 10.1594/PANGAEA.855539).

[1]To whom correspondence should be addressed. Email: roelof@geod.uni-bonn.de.

This article contains supporting information online at www.pnas.org/lookup/suppl/doi:10.1073/pnas.1519132113/-/DCSupplemental.

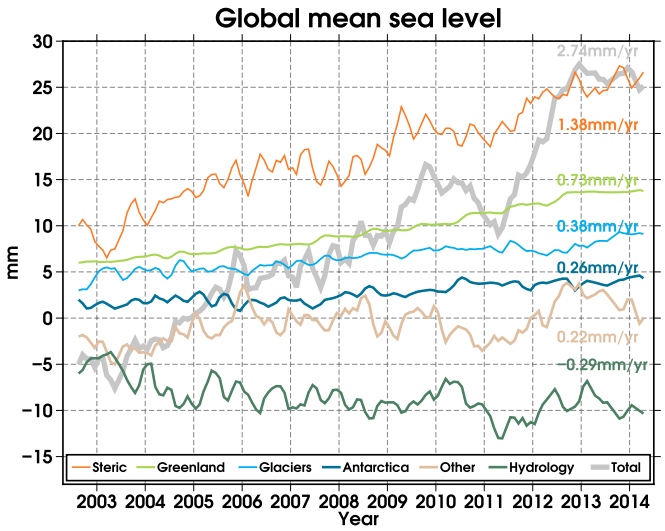

Fig. 1. Global mean relative sea level, divided into different contributions. Annual and semiannual harmonics have been fitted and removed and the resulting curves are smoothed with a 3-month running mean (trends are derived from the unsmoothed data). The curves have been offset for clarity.

gravimetric observations from GRACE, over the period 2002 (April)–2014 (June). An additional nonrandom, deterministic sea-level component is estimated, which is used to separate remaining signals in large-scale sea level, e.g., residual mass variations due to ocean circulation, from observational noise. The sea-level budget is considered globally and for a set of dedicated coastal zones (see the colored polygons in Fig. 2). Our simultaneous least-squares inversion allows for a consistent closure of the sea-level budget, taking into account technique errors and coverage (*Materials and Methods* and *SI Appendix*). Another advantage is that no additional filtering of the GRACE data is required in our method. Such filtering is commonly applied to reduce the typical north–south errors of the GRACE products, but it attenuates the spatial content of the signal, with a decrease of spatial resolution as a result.

Global Mean Sea-Level Budget

The different contributions to global mean relative sea-level rise are computed by aggregating the relevant inversion results and are plotted in Fig. 1. In addition, trends, significant accelerations, annual amplitudes and phases are tabulated in Table 1.

Striking is that the estimated steric sea-level trend, 1.38 ± 0.16 mm/y (April 2002–June 2014 or 1.36 mm/y over April 2002–December 2012), is significantly larger compared with an independent estimate obtained from the upper 1,500 m of the ocean, which stands at 0.66 ± 0.17 mm/y (using gridded in situ data from ref. 20 over the period 2002–2012). In another study, an even smaller steric trend derived from Argo data indicates 0.5 ± 0.1 mm/y (2005–2012) of thermosteric sea level in the first 1,500 m, where it must be noted that Argo potentially underestimates steric sea-level trends due to sampling problems (19). Similarly, the thermosteric component of sea level in the first 2,000 m has been estimated at 0.54 mm/y (21) (1955–2010).

In the abyssal ocean (below 4,000 m), a significant thermosteric warming trend of 0.053 ± 0.017 mm/y has been found over the 1990s and 2000s, with an additional 0.093 ± 0.081 mm/y, when the Southern Ocean between 1,000 and 4,000 m is considered too (22). Somewhat later, a steric trend of 0.095 mm/y for the layers below 3,000 m has been found from observations (23). However, in light of our results, the trend in the first 1,500 m and in the abyssal ocean cannot explain the 1.39 mm/y we found from the GRACE and altimetry data.

The operational ocean reanalysis system (ORAS4), assimilating various hydrographic datasets and altimetry, can provide estimates of the steric trend in the entire ocean column (24). Over the time period considered here, global mean thermosteric and halosteric trends of 1.43 mm/y and −0.53 mm/y (combined 0.94 mm/y) are derived, respectively, from the ORAS4 data (see also Table 1). It is interesting to note that the thermosteric trend from ORAS4 is much more consistent with our estimate, especially when considering that the strong negative halosteric trend is considered spurious and linked to the assimilation of recent Argo data (24).

GIA has no direct contribution in terms of mean relative sea level, although it indirectly does significantly influence the estimate for the Antarctic mass loss contribution. It is common to

Table 1. Estimated annual amplitudes, phases (indicating day of maximum), trends, and accelerations of the different contributions to global mean sea level in the period 2002–2014

	Annual		Trend	Acceleration	rms
Contribution	A, mm	t_a, doy	mm/y	mm/y^2	post., mm
Gr + An + Gl	1.3 (± 0.36)	281 (± 17)	1.37 (± 0.09)	0.03 (± 0.019)	0.9
Antarctica	0.3 (± 0.18)	83 (± 32)	0.26 (± 0.04)	0.01 (± 0.009)	0.6
Greenland	0.5 (± 0.07)	285 (± 8)	0.73 (± 0.02)	0.02 (± 0.004)	0.3
Glaciers	1.2 (± 0.25)	276 (± 14)	0.38 (± 0.07)	—	0.6
Hydrology	11.0 (± 0.98)	270 (± 6)	−0.29 (± 0.26)	—	1.9
Steric	4.6 (± 0.71)	51 (± 9)	1.38 (± 0.16)	—	1.7
Other	3.3 (± 1.03)	82 (± 20)	0.22 (± 0.26)	—	2.0
Total	6.1 (± 2.20)	303 (± 22)	2.74 (± 0.58)	—	2.7
Steric (Ishii, 1,500m)	3.6 (± 0.76)	87 (± 12)	0.66 (± 0.17)	—	1.2
Thermo	3.4 (± 1.08)	94 (± 18)	0.59 (± 0.25)	—	1.1
Halo	0.4 (± 0.30)	18 (± 42)	0.07 (± 0.07)	—	1.1
Steric (ORAS4)	3.6 (± 0.38)	80 (± 6)	0.94 (± 0.08)	—	1.2
Thermo	3.2 (± 0.44)	78 (± 8)	1.43 (± 0.09)	—	1.0
Halo	3.7 (± 0.28)	79 (± 4)	−0.53 (± 0.05)	—	0.9

The estimate from Ishii and Kimoto (20) only contains data up to Dec. 2012. Accelerations are only estimated when significant (1-σ). The last column denotes the rms of the residuals. doy, day of year.

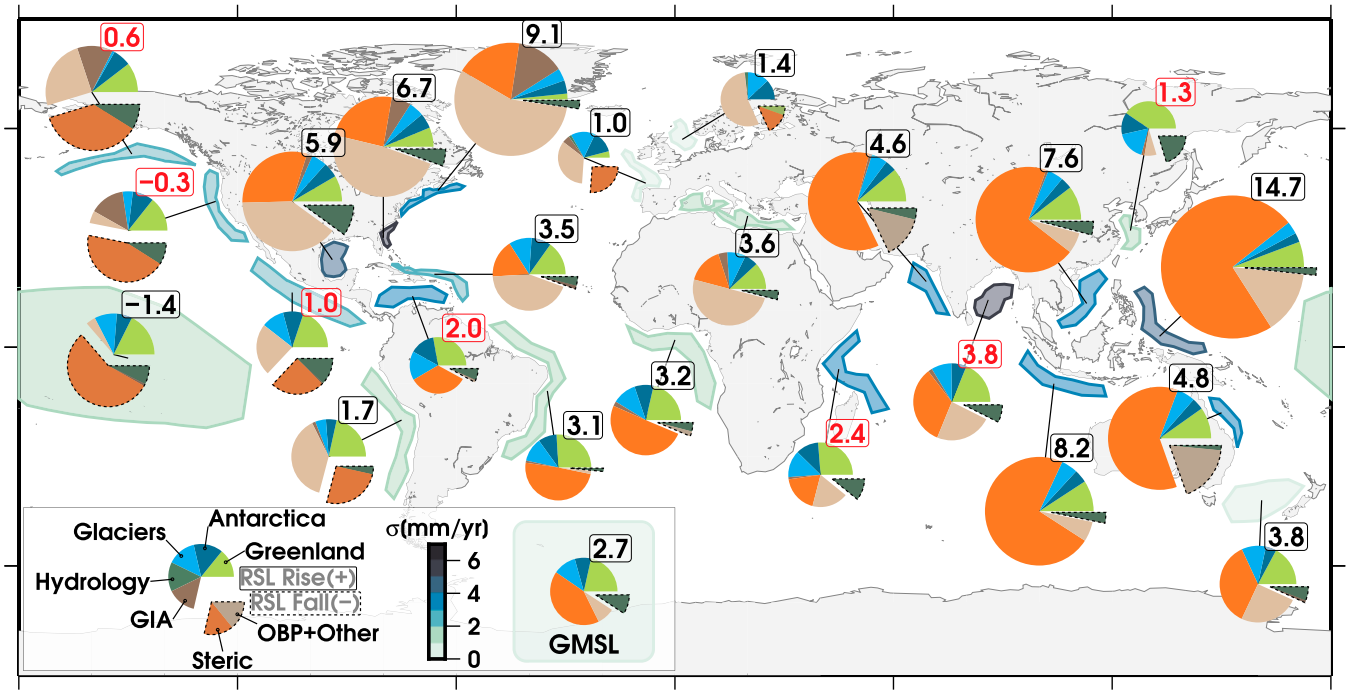

Fig. 2. Relative sea-level rise in mm/y in selected coastal zones. The associated polygons are colored according to the estimated total error (*Materials and Methods*). Wedge areas reflect the absolute magnitude of the different contributions, and negative wedges are shaded. Trends with red numbers indicate nonsignificant (1-σ) total trends, although the individual components may have significant contributions (*SI Appendix*, Table S4).

subtract a GIA correction of −0.3 mm/y from the altimetry record (e.g., ref. 25) to convert from global mean geocentric sea level to relative sea level. From the estimated GIA signal from this study, we find a smaller correction (−0.1 mm/y). To put this number into perspective, compared with an ensemble of GIA runs from (26), our estimate lies at the upper bound of the spread of the GIA models (−0.1 to −0.5 mm/y). This smaller correction can be partly explained by a weaker GIA signal found in the Antarctic (*SI Appendix*, Tables S1 and S2), implying a decreased mantle flow from the ocean basin to the Antarctic continent, which in its turn causes a smaller volumetric change of the mean ocean basin. A relatively weak present-day GIA signal in the Antarctic is also confirmed by 3D Earth models (27).

Fig. 1 and Table 1 also show that some components exhibit considerable interannual variations. The residual variations, 3.3 mm in terms of root-mean-square (rms), are mostly determined by the hydrological, steric, and "other" component (*Materials and Methods*). The contribution of Greenland to sea level contains the smallest residual variations (0.3-mm rms), indicating the robustness of its mass loss signal. Besides the trend, 0.73 mm/y, a significant acceleration of about 0.02 ± 0.004 mm/y^2, can also be found over the considered period.

Table 1 indicates that the annual steric sea level (peaking end of February) is partly compensated by the hydrological component (reaches its minimum in the end of March), similar to what has been observed by ref. 28.

Regional Sea-Level Budget

The regional contributions differ significantly from those of the global mean sea level. For a selection of coastal zones (the inversion results have been evaluated in areas as indicated by colored polygons), regional sea-level trends and their contributions are graphically depicted in Fig. 2 (trends are tabulated in *SI Appendix*, Table S4). The coastal zones were selected to cover a wide set of different characteristics [e.g., vulnerability (2), occurrence of upwelling regions, coastal shelves]. To avoid contamination by land effects, and errors from interpolation of steric fields, the regions have been hand-drawn while avoiding regions with too much variations in the altimetric sea level. It should be noted that effects from local subsidence and tectonics are not considered in this study, but these may be added for local studies. In the western Pacific and Indian Ocean, sea-level rise is dominated by the steric contribution (up to 75%), most notably the 14.7 ± 4.4-mm/y rise in the vicinity of the Philippines, and trends of 7.6 ± 3.17 mm/y (South China Sea) and 8.3 ± 4.7 mm/y (Indonesia). At the same time, the contribution from glaciers and ice sheets (Gr + An + Gl) is also relatively strong as these coastlines are positioned far away from the melting sources. On the other hand, negative steric contributions (down to -2.8 ± 1.5 mm/y) are found in the central and eastern part of the Pacific.

For most coastlines, in particular around the Atlantic Ocean, we find significant contributions which cannot be explained by

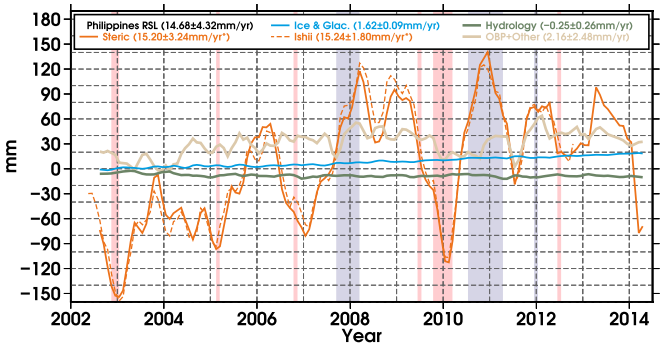

Fig. 3. Time-variable sea-level contributions to the east of the Philippines. Warm (El Niño, red) and cold (La Niña, blue) phases are highlighted whenever the MEI gets larger than 1 or smaller than −1, respectively. The asterisk indicates that the trend is computed over the period where there are Ishii data available (2002–2012). Plots of other regions can be found in the *SI Appendix*.

either steric changes or land–ocean mass exchange (indicated by OBP + other in the figures and tables, where "OBP" is ocean bottom pressure). For example, near the east coast of the United States and in the North Sea, more than 50% of the trend is attributed to the "OBP + other" component. On regional scales, this contribution is expected to be strongly influenced by internal mass variations of the ocean (e.g., bottom pressure change caused by wind stress forcing) (29, 30). In the deeper parts of the ocean it is also possible that these reflect remaining steric signal which cannot be absorbed by the chosen parameterization of the steric parameters (*SI Appendix*).

For most coastlines, the hydrological contribution is found to be zero or negative (the lowest component amounts to -0.7 ± 0.27 mm/y in the Gulf of Mexico).

Compared with other contributions, GIA-related relative sea level remains fairly small, except for regions closer to the former ice sheets. The largest GIA trends (1.3 ± 0.25 mm/y) take place in the coastal zone at the northeast United States, which is located on the subsiding peripheral bulge of the former Laurentide ice sheet.

Accelerations and Interannual Changes at Regional Scales

Regional sea-level variations are generally more variable compared with the global mean. The trends provided in this paper are based on a short timespan (2002–2014) because of the limited availability of GRACE data. Uncertainties in the trends are based on empirical autoregressive models of order 1 and therefore reflect mainly the correlated interannual signals in the residuals. To visualize the interannual variability of the different contributions, we have plotted the time-varying components of sea level in Fig. 3 for the case of the Philippines. Plots of the other zones can be found in the *SI Appendix*.

Fig. 3 shows that the steric component and the component related to OBP and other signals contain by far the strongest interannual signals. In stark contrast stand the much smoother contributions from the ice sheets, glaciers, and hydrology. Consequently, the accuracy of the sea-level trend, and the ability to extrapolate such trends in the future, is severely limited by variations of the steric contribution. It is well known that total (global and regional) sea level is sensitive to large interannual variations, such as the El Niño Southern Oscillation (ENSO) (31, 32). This can also be seen in Fig. 3. A regression with the Multivariate ENSO Index (MEI) removes 30% of the SD of the steric series (maximum correlation occurred at zero lag), but a significant interannual component remains nonetheless and cannot be easily explained by the ENSO.

For other coastal zones, it can generally be said that interannual variations in the steric component are the main cause of uncertainties in the trends. One exception is the North Sea, where the shallow water column cannot accommodate large steric variations. Consequently, components related to wind stress and other effects introduce the largest interannual variations that play a larger role there.

Discussion

The simultaneous combination of sea-level anomalies from satellite altimetry and data from satellite gravimetry allows a partitioning of the sea-level rise into the different contributions. The estimated global mean sea-level rise over the past 12 y (2002–2014) amounts to 2.74 ± 0.58 mm/y, which can be attributed to glaciers and ice sheets (1.37 ± 0.09 mm/y), terrestrial hydrology (-0.29 ± 0.26 mm/y), steric sea-level rise (1.38 ± 0.16 mm/y), and a remaining nonrandom component of 0.22 ± 0.26 mm/y, which is needed to close the global mean sea-level budget. The enigma is that the steric component is more than two times as large compared with the estimate derived from hydrographic data from the first 1,500 m in the ocean (0.66 ± 0.17 mm/y), and is also larger than other similar estimates of steric sea-level rise (19, 21). It has to be mentioned that signals in the deeper ocean (1,500-m bottom) and in regions not frequently visited by Argo floats are not well resolved by the hydrographic data, and may potentially cause a low bias (19), although it is commonly expected that warming at intermediate depths is relatively small (33). Furthermore, although the halosteric signal should not give rise to large steric signals, salinity errors may potentially influence the steric trends as well.

Another possibility is that the inversion scheme used here significantly underestimates the combined mass losses from the major ice sheets, glaciers, and hydrology. This leads to the larger steric trend, because the closure of the sea-level budget is respected in the inversion. Using an ocean basin averaging technique, another study found a significantly larger mass trend from GRACE data (2.0 ± 0.1 mm/y) over a shorter period (2005–2013) (15). However, we would like to emphasize that the smaller mass trend we found here (1.08 ± 0.3 mm/y) is consistent with published estimates of mass loss in the ice sheets, glaciers, and hydrology. For Greenland we find -270 ± 7 Gt/y, which is comparable to -230 ± 33 Gt/y (34), and more recently -278 ± 19 Gt/y (17). For Antarctica, our estimate (-96 ± 15 Gt/y) is consistent with the most recent estimates which use smaller GIA corrections [-92 ± 26 Gt/y (17) and -114 ± 23 Gt/y (35)]. Furthermore, land glaciers (in this study -141 ± 26 Gt/y) agree within the error bars with the -148 ± 30 Gt/y found in ref. 36. Finally, the remaining hydrological contribution to sea level is slightly negative (here -0.29 ± 0.26 mm/y) and agrees with the -0.22 ± 0.05 mm/y from ref. 9, and -0.1 ± 0.3 mm/y (8) (see *SI Appendix*, Table S3 for additional comparisons).

The interannual variability of the steric and hydrological component is responsible for about 50% of the interannual variations of the total sea level; this is in line with ref. 37, which used hydrologic and steric corrections to reduce the interannual variability of the global mean sea level.

On regional scales, the relative contributions to the sea-level budget depend strongly on the coastline location (see also *SI Appendix*, Table S4). The most extreme case can be found at the Philippines, where a trend of 14.7 ± 4.4 mm/y was found. The steric component is largely responsible for this rate (11.2 ± 3.6 mm/y).

On the other hand, negative rates have been found in the Central Pacific and at the west coast of the United States.

At regional scales, we find significant components which cannot be simply attributed to steric changes or land–ocean mass exchange. These trends are most likely related to trends in the OBP, but may also contain residual steric signals. This holds in particular for coastlines bordering the North Atlantic. It is known that in shallow regions such as the North Sea, wind-driven Ekman transport plays a large role at decadal scales (11). Although its magnitude depends on the location, the trends from glaciers and ice sheets exhibit a relatively smooth and similar behavior over time, and an acceleration over the last decade can be observed at the majority of the coastlines.

Although the time period of this study is still relatively short, we expect that the observational results from this study are important for model validation and identifying regional sea-level drivers. Because our inversion results are not dependent on data from Argo floats and other hydrographic data, they shed new light on the discussion of "missing heat" in the Earth system (38–40) and the consistent closure of the sea-level budget.

Materials and Methods

Inversion Methodology. In our forward modeling–least-squares approach (41, 42), the different contributions are parameterized by predefined spatial patterns, each scaled with an unknown time-varying magnitude. The spatial information for each pattern, coined "fingerprints," originates from a priori data, whereas the time evolution is estimated from altimetry and GRACE data. In this study, 200 empirical orthogonal functions (EOF) are used as steric sea-level fingerprints. These are computed from integrating, over the full ocean column, volume changes from temperature and salinity variations from the Finite Element Sea Ice–Ocean Model (FESOM) (10, 43), and explain more than 99% of the modeled variance of steric sea level. Because FESOM

uses variable-size finite elements, it is possible to obtain steric values close to the coast, and in shallow areas. These steric heights are then interpolated on a 0.5 × 0.5-degree grid, which is used as input for the EOF analysis (area-weighted).

Continental hydrological mass changes, and mass variations of the glaciers and ice sheets (Gr + An + Gl) are discretized by 119 global patterns, which include a passive ocean response, mass-consistent with the applied land load and accounting for the effect of rotational feedback (see *SI Appendix* for the discretization used). This involves solving the so-called "Sea-Level Equation" (44), which, in our case, is performed in the spherical harmonic domain (41, 45). In addition, contributions from five separate GIA patterns, each representing the effect of a former glacial mass (Laurentide, Antarctica, Greenland, Fennoscandia, and auxiliary glacial masses), are used as fingerprints. To account for possible frame offsets of the radar altimeters, satellite-specific unconstrained mean reference system offsets are introduced and solved for simultaneously.

After the initial inversion step, significant large-scale geophysical residuals remain in the altimetry residuals. We therefore decided to fit an additional set of fingerprints to the data, to separate unexplained but significant nonrandom sea-level signals from pure noise. These fingerprints are constructed by extracting the 100 leading EOF modes of the gridded and Gaussian-smoothed (200-km half width) altimetry residuals from the first inversion step. In the final inversion step, these parameters are then estimated together with the other parameters. Throughout the paper, this component is referred to as "other," as it contains a mix of signals (deep and shallow steric changes, which are not accounted for by the steric fingerprints, and internal ocean mass variations as deviations from the background model).

Sea-Level Anomalies. To link the sought-for parameters to the binned along-track sea-level anomalies, $\delta \boldsymbol{h}_{sla}$, we consider the following observation equation:

$$\delta \boldsymbol{h}_{sla}(t) = \mathbf{YB}\begin{bmatrix} \boldsymbol{x}_{ice}(t) \\ \boldsymbol{x}_{glac}(t) \\ \boldsymbol{x}_{hydro}(t) \\ (t-t_0)\boldsymbol{x}_{gia} \end{bmatrix} + \mathbf{KC}\begin{bmatrix} \boldsymbol{x}_{steric}(t) \\ \boldsymbol{x}_{other}(t) \end{bmatrix} + \mathbf{P}[\boldsymbol{x}_{satbias}] + \varepsilon. \quad [1]$$

The vector $\boldsymbol{x}_{\_}$ contains the monthly contributions of the ice sheets, glaciers, hydrology, and steric heights. In contrast to those, the GIA parameters, $\boldsymbol{x}_{gia}$, and the altimeter-specific offsets, $\boldsymbol{x}_{satbias}$, are estimated with data over the entire timespan as they are modeled as trends and a bias, respectively (42). The computed fingerprints, expressed in terms of geocentric sea level, are contained in matrix **B** and **C**. The fingerprints in **B** are expressed in terms of spherical harmonic coefficients, which are mapped to the altimeter tracks with matrix **Y**. The steric EOF modes from FESOM are provided on 0.5 × 0.5-degree grids, which are bilinearly interpolated to the altimeter tracks using matrix **K**. Matrix **P** projects the satellite offset onto the radial direction of the measurement.

Along-track radar altimetry data are taken from the Radar Altimeter Database System [RADS (46)], and averaged into along-track bins of about 1-s length (roughly 6 km). All standard range corrections are applied to the data before averaging, and large outliers are removed.

Satellite Gravimetry. Similarly, the observation equation for the GRACE Stokes coefficients, $\delta \boldsymbol{C}$, looks like

$$\delta \boldsymbol{C}(t) = \boldsymbol{D}\begin{bmatrix} \boldsymbol{x}_{ice}(t) \\ \boldsymbol{x}_{glac}(t) \\ \boldsymbol{x}_{hydro}(t) \\ (t-t_0)\boldsymbol{x}_{gia} \end{bmatrix} + \varepsilon. \quad [2]$$

Obviously, no steric changes can be observed by GRACE and Eq. **2** is described in the spherical harmonic domain. The columns of matrix **D** contain the fingerprints, but are here expressed in terms of Stokes coefficients. In this study, we have used monthly GRACE RL05 data processed by the GFZ German Research Centre for Geosciences (47). The data are provided in the form of full (unsolved) normal equation systems, expressed in terms of residual Stokes coefficients, from which we use the information up to spherical harmonic degree and order 150. These systems are transformed with matrix **D** while avoiding an intermediate (ill-posed) solving step (42).

Background Model. Besides the standard corrections, both the GRACE data and altimetry have been reduced with modeled variations of monthly averaged OBP variations [ECMWF + OMCT (48)]. Here, we use the ocean–atmosphere product (GAC) from the GRACE standard processing, except that we apply an additional monthly correction over the ocean, which ensures that the background model contains no mean ocean signal for each time step. OBP variations from the background model, OBP_{GAC}, are thus modified over the ocean domain (ocean function O) to obtain OBP^*_{GAC}:

$$OBP^*_{GAC}(\omega, t) = OBP_{GAC}(\omega, t) - \frac{O(\omega)}{A_{oce}} \int_{Ocean} OBP_{GAC}(\omega, t) d\omega. \quad [3]$$

Because the GRACE normal equation systems are already reduced with the GRACE dealiasing product, we only need to update the background model with the last term above.

Regional Trend Correction. It was found that the background model introduces spurious regional sea-level trends, which consequently contaminate trends in the regional inversion results. To mitigate this, we restored the trends of OBP^*_{GAC} to the "other" component of the inversion in a post-processing step. The resulting component, denoted as OBP + other, therefore additionally reflects the complete OBP trend signal. This correction is not necessary for the global mean estimates, as the ocean mean of OBP^*_{GAC}, and consequently its trend is zero per definition.

External Steric Sea Level. For the computation of the external estimate of the steric height evolution, we use temperature and salinity data from ref. 20 (V6.13) in the first 1500m of the ocean, in combination with the thermodynamic equation of seawater (TEOS) (49).

Constraints. During the solving step, two types of (weak) constraints are needed to avoid instabilities in the solution (see also the *SI Appendix*). The first is a Tikonov constraint which pushes the GIA secular scale factors toward the a priori GIA model. The other constraint is applied to selected combinations of small and neighboring ice sheet drainage basins, and constrains the equivalent water height in them toward a common value.

Error Estimates. Although we propagate instrumental errors from GRACE and altimetry (range errors) to the sea-level heights, these are unrealistically small because of the dramatic reduction of the solution space (only 400 parameters are estimated each month compared with >10,000 gravity coefficients). For the error estimates of the trends and seasonal components, we therefore use empirical autoregressive models of order 1, which are computed from the postfit residuals of each time series. The errors therefore also reflect correlated errors in time, which arise due to interannual variability.

Errors in the secular GIA component are even harder to quantify, especially because we apply constraints. We decided to apply a worst-case error, where we took the magnitude of the estimated GIA corrections itself, and applied it as an error. Although we believe that the data do have some resolving power and this error is too large, it does reflect the spread in current GIA models.

Global Mean Sea Level and Coastal Zones. To estimate a time-varying contribution for the mean sea level, $s(t)$, we compute from the estimated and relevant components, x_i:

$$s(t) = \sum_i N_i x_i(t), \quad [4]$$

where the time-invariant factors N_i correspond to the ocean average of the associated fingerprint, which can be found from matrices B and C (using an area-weighted average).

For the regional coastline estimates, we evaluate the inversion results in terms of relative sea level as area averages over the hand-drawn polygons shown in Fig. 2. Mass components and GIA are evaluated as spectral basin averages (the results have been validated with spatial methods), whereas the gridded components were obtained by area weighting the cells in the region.

ACKNOWLEDGMENTS. We thank three reviewers whose comments improved the manuscript considerably. Magdalena Balmaseda is thanked for providing global mean steric trends from the ORAS4 model. Valentina Barletta is thanked for providing modeled glacial isostatic adjustment (GIA) trends from her ensemble runs. Furthermore, we are grateful to Volker Klemann for providing the GIA modeling results, and thank the German Space Operations Center of the German Aerospace Center for providing continuously and nearly 100% of the raw telemetry data of the twin GRACE satellites. We also acknowledge Radar Altimeter Database System (RADS) for providing up-to-date and flexible along-track altimetry products. All figures are made using the Generic Mapping Tools. This research has been funded by the German Research Foundation under Grants KU1207/9-2 and SCHR779/6-2 and by the German Federal Ministry of Education and Research Support Code 03F0654A.

1. Stocker TF, et al. (2013) Climate change 2013: The physical science basis. *Intergovernmental Panel on Climate Change, Working Group I Contribution to the IPCC Fifth Assessment Report (AR5)* (Cambridge Univ Press, New York).
2. Nicholls RJ, Cazenave A (2010) Sea-level rise and its impact on coastal zones. *Science* 328(5985):1517–1520.
3. Church JA, White NJ (2011) Sea-level rise from the late 19th to the early 21st century. *Surv Geophys* 32(4):585–602.
4. Hay CC, Morrow E, Kopp RE, Mitrovica JX (2015) Probabilistic reanalysis of twentieth-century sea-level rise. *Nature* 517(7535):481–484.
5. Jevrejeva S, Moore J, Grinsted A, Woodworth P (2008) Recent global sea level acceleration started over 200 years ago? *Geophys Res Lett* 35(8):L08715.
6. Jensen L, Rietbroek R, Kusche J (2013) Land water contribution to sea level from Grace and Jason-1 measurements. *J Geophys Res: Oceans* 118(1):212–226.
7. Chao BF, Wu YH, Li YS (2008) Impact of artificial reservoir water impoundment on global sea level. *Science* 320(5873):212–214.
8. Riva REM, Bamber JL, Lavallée DA, Wouters B (2010) Sea-level fingerprint of continental water and ice mass change from grace. *Geophys Res Lett* 37(19):L19605.
9. Llovel W, Becker M, Cazenave A, Crétaux J-F, Ramillien G (2010) Global land water storage change from Grace over 2002–2009; inference on sea level. *C R Geosci* 342(3): 179–188.
10. Brunnabend S-E, Schröter J, Timmermann R, Rietbroek R, Kusche J (2012) Modeled steric and mass-driven sea level change caused by Greenland ice sheet melting. *J Geodyn* 59-60:219–225.
11. Dangendorf S, Calafat FM, Arns A, Wahl T, Haigh ID, Jensen J (2014) Mean sea level variability in the north sea: Processes and implications. *J Geophys Res: Oceans* 119(10): JC009901.
12. Cazenave A, Llovel W (2010) Contemporary sea level rise. *Annu Rev Mar Sci* 2:145–173.
13. Lombard A, et al. (2007) Estimation of steric sea level variations from combined Grace and Jason-1 data. *Earth Planet Sci Lett* 254(1):194–202.
14. Gregory J, et al. (2013) Twentieth-century global-mean sea level rise: Is the whole greater than the sum of the parts? *J Clim* 26(13):4476–4499.
15. Llovel W, Willis J, Landerer F, Fukumori I (2014) Deep-ocean contribution to sea level and energy budget not detectable over the past decade. *Nat Clim Change* 4(11): 1031–1035.
16. Chen J, Wilson C, Tapley B (2013) Contribution of ice sheet and mountain glacier melt to recent sea level rise. *Nat Geosci* 6(7):549–552.
17. Schrama E, Wouters B, Rietbroek R (2014) A mascon approach to assess ice sheet and glacier mass balances and their uncertainties from Grace data. *J Geophys Res: Solid Earth* 119(7):6048–6066.
18. Holgate SJ, et al. (2012) New data systems and products at the permanent service for mean sea level. *J Coast Res* 29(3):493–504.
19. Von Schuckmann K, et al. (2013) Monitoring ocean heat content from the current generation of global ocean observing systems. *Ocean Sci Discuss* 10:923–949.
20. Ishii M, Kimoto M (2009) Reevaluation of historical ocean heat content variations with time-varying XBT and MBT depth bias corrections. *J Oceanogr* 65(3):287–299.
21. Levitus S, et al. (2012) World ocean heat content and thermosteric sea level change (0–2000 m), 1955–2010. *Geophys Res Lett* 39(10):L10603.
22. Purkey SG, Johnson GC (2010) Warming of global abyssal and deep southern ocean waters between the 1990s and 2000s: Contributions to global heat and sea level rise budgets. *J Clim* 23(23):6336–6351.
23. Kouketsu S, et al. (2011) Deep ocean heat content changes estimated from observation and reanalysis product and their influence on sea level change. *J Geophys Res: Oceans (1978–2012)* 116(C3):C03029.
24. Balmaseda MA, Trenberth KE, Källén E (2013) Distinctive climate signals in reanalysis of global ocean heat content. *Geophys Res Lett* 40(9):1754–1759.
25. Nerem R, Chambers D, Choe C, Mitchum G (2010) Estimating mean sea level change from the Topex and Jason altimeter missions. *Mar Geod* 33(S1):435–446.
26. Barletta VR, Sorensen LS, Forsberg R (2013) Scatter of mass changes estimates at basin scale for Greenland and Antarctica. *The Cryosphere* 7(5):1411–1432.
27. van der Wal W, Whitehouse PL, Schrama EJ (2015) Effect of GIA models with 3D composite mantle viscosity on GRACE mass balance estimates for Antarctica. *Earth Planet Sci Lett* 414:134–143.
28. Chen J, Wilson C, Tapley B, Chambers D, Pekker T (2001) Hydrological impacts on seasonal sea level change. *Global Planet Change* 32(1):25–32.
29. Bonin JA, Chambers DP (2011) Evaluation of high-frequency oceanographic signal in Grace data: Implications for de-aliasing. *Geophys Res Lett* 38(17):L17608.
30. Johnson GC, Chambers DP (2013) Ocean bottom pressure seasonal cycles and decadal trends from GRACE release-05: Ocean circulation implications. *J Geophys Res: Oceans* 118(19):4228–4240.
31. Böning C, Willis JK, Landerer FW, Nerem RS, Fasullo J (2012) The 2011 La Niña: So strong, the oceans fell. *Geophys Res Lett* 39:L19602.
32. Cazenave A, et al. (2012) Estimating ENSO influence on the global mean sea level, 1993–2010. *Mar Geod* 35:82–97.
33. Dieng HB, Palanisamy H, Cazenave A, Meyssignac B, von Schuckmann K (2015) The sea level budget since 2003: Inference on the deep ocean heat content. *Surv Geophys* 36(2):209–229.
34. Velicogna I (2009) Increasing rates of ice mass loss from the Greenland and Antarctic ice sheets revealed by Grace. *Geophys Res Lett* 36(19):L19503.
35. Sasgen I, et al. (2013) Antarctic ice-mass balance 2003 to 2012: Regional reanalysis of GRACE satellite gravimetry measurements with improved estimate of glacial-isostatic adjustment based on GPS uplift rates. *The Cryosphere* 7:1499–1512.
36. Jacob T, Wahr J, Pfeffer WT, Swenson S (2012) Recent contributions of glaciers and ice caps to sea level rise. *Nature* 482(7386):514–518.
37. Cazenave A, et al. (2014) The rate of sea-level rise. *Nat Clim Change* 4:358–361.
38. Trenberth KE, Fasullo JT (2010) Climate change. Tracking Earth's energy. *Science* 328(5976):316–317.
39. Lyman JM, et al. (2010) Robust warming of the global upper ocean. *Nature* 465(7296): 334–337.
40. Loeb N, et al. (2012) Observed changes in top-of-the-atmosphere radiation and upper-ocean heating consistent within uncertainty. *Nat Geosci* 5(2):110–113.
41. Rietbroek R, Brunnabend SE, Kusche J, Schröter J (2012) Resolving sea level contributions by identifying fingerprints in time-variable gravity and altimetry. *J Geodyn* 59:72–81.
42. Rietbroek R (2014) Retrieval of sea level and surface loading variations from geodetic observations and model simulations: An integrated approach. PhD thesis (University of Bonn, Bonn, Germany).
43. Timmermann R, et al. (2009) Ocean circulation and sea ice distribution in a finite element global sea ice-ocean model. *Ocean Model* 27(3):114–129.
44. Woodward R (1888) On the form and position of mean sea level. *Geol Surv Bull* 48: 87–170.
45. Dahlen FA (1976) The passive influence of the oceans upon the rotation of the earth. *Geophys J R Astron Soc* 46(2):363–406.
46. Scharroo R, et al. (2013) RADS: Consistent multi-mission products. *Proceedings of the Symposium on 20 Years of Progress in Radar Altimetry, Venice, 20–28 September 2012, ESA SP-710* (ESA, Noordwijk, The Netherlands). Vol 20.
47. Dahle C, et al. (2013) *GFZ GRACE Level-2 Processing Standards Document for Level-2 Product Release 12/02 - Data* (Deutsches GeoForschungsZentrum GFZ, Potsdam, Germany), Scientific Technical Report STR12/02 – Data, Revised Ed, January 2013.
48. Dobslaw H, et al. (2013) Simulating high-frequency atmosphere-ocean mass variability for dealiasing of satellite gravity observations: AOD1B RL05. *J Geophys Res: Oceans* 118(7):3704–3711.
49. McDougall TJ, Barker P (2011) Getting started with TEOS-10 and the Gibbs seawater (GSW) oceanographic toolbox. SCOR/IAPSO WG 127:1–28. Version 3.

Supplementary Material

Supplementary Material to:
Revisiting the Contemporary Sea Level Budget on Global and Regional Scales
Authors:
Roelof Rietbroek, Sandra-Esther Brunnabend, Jürgen Kusche, Jens Schröter, Christoph Dahle
The data used for this paper can be downloaded from the Pangaea Archive:
http://dx.doi.org/10.1594/PANGAEA.855539

Joint inversion weighting scheme

For completeness we describe here how the different datasets are combined in the joint inversion (see also [1]).

Altimetry
For each month we create for every altimetry satellite a normal equation system:

$$N_{Jasonx}(t)\,\mathbf{x}(t) = \mathbf{b}_{Jasonx}(t)\,,\ _{x=1,2} \tag{s1}$$

The to-be-solved-for solution vector $\mathbf{x}$ contains vectors of the individual elements:

$$\mathbf{x} = \begin{bmatrix} x_{ice} \\ x_{glac} \\ x_{hydro} \\ x_{gia} \\ x_{steric} \\ x_{other} \\ x_{satbias} \end{bmatrix} \tag{s2}$$

The normal matrix, N_{Jasonx}, can be computed from the observation equation (equation 1 from the main paper) as:

$$N_{Jasonx}(t) = \begin{bmatrix} B^T Y^T & C^T K^T \end{bmatrix} C^{-1}_{Jasonx}(t) \begin{bmatrix} YB \\ KC \end{bmatrix} \tag{s3}$$

Where we use a diagonal error-covariance matrix, C_{Jasonx}, which is constructed from the range errors provided by the radar altimeters (derived from the noise of the 20Hz data).

The right hand side of the normal equation system is computed as:

$$\mathbf{b}_{Jasonx}(t) = \begin{bmatrix} B^T Y^T & C^T K^T \end{bmatrix} C^{-1}_{Jasonx}(t) \left(\delta h^{Jasonx}_{sla}(t,\theta,\lambda) - OBP^*_{GAC}(\theta,\lambda) \right) \tag{s4}$$

The sea level anomalies were already corrected with a high frequency (< 10days) dynamic atmospheric correction (DAC), but we additionally reduce the signal for monthly averages of our Ocean Atmosphere correction (see equation 3 of the main article), in order to be consistent with the GRACE processing.

GRACE
The GRACE data is provided in terms of normal equation systems, expressed in normalized Stokes coefficients. From the systems we eliminate (i.e. solve implictly [2]) auxiliary parameters, such as initial orbit state vectors, and accelerometer scales, until we are left with a system which is linked to the vector of monthly Stokes coefficients, $\phi_{nm}(t)$ up to degree and order 150:

$$N_{\phi}(t)\,\phi_{nm}(t) = \mathbf{b}_{\phi}(t) \tag{s5}$$

The signal in this system of equation is already reduced with the standard GRACE dealiasing product, but also with trends, and (semi)annual harmonics derived from the EIGEN-6c static gravity field model. To make the data consistent with altimetry we therefore need to apply a small update to the right hand side vector of the system:

$$\mathbf{b}^*_{\phi} = \mathbf{b}_{\phi} - N_{\phi}\delta\phi_{nm}(t) \tag{s6}$$

The update vector $\delta\phi_{nm}(t)$ contains Stokes coefficients with a contribution from the ocean mean of the monthly GAC product (right hand side of equation 3 of the main article), and an additional component which is used to restore the time variable part of the EIGEN-6c model.

This system can now be transformed into a system expressed in our parameters of interest $\mathbf{x}$ by:

$$N_{GRACE}(t) \begin{bmatrix} x_{ice} \\ x_{glac} \\ x_{hydro} \\ x_{gia} \end{bmatrix} = \mathbf{b}_{GRACE}(t) \tag{s7}$$

Where we use the observation equation 2 from the main article to convert the normalmatrix and right hand side:

$$N_{GRACE}(t) = B^T N_{\phi} B \tag{s8}$$

$$\mathbf{b}_{GRACE}(t) = B^T \mathbf{b}^*_{\phi} \tag{s9}$$

Variance Component Estimation
When combining normal equation systems from GRACE and altimetry we allow their error-covariance to be scaled by a scalar variance component. This will absorb systematic over- or underestimation of the formal error covariance, which may occur in different observation techniques.

$$N_{comb}(t) = \frac{1}{\sigma^2_{GRACE}} N_{GRACE} + \frac{1}{\sigma^2_{Jason1}} N_{Jason1} + \frac{1}{\sigma^2_{Jason2}} N_{Jason2} \tag{s10}$$

$$\mathbf{b}_{comb}(t) = \frac{1}{\sigma^2_{GRACE}} \mathbf{b}_{GRACE} + \frac{1}{\sigma^2_{Jason1}} \mathbf{b}_{Jason1} + \frac{1}{\sigma^2_{Jason2}} \mathbf{b}_{Jason2} \tag{s11}$$

In this study we estimate the variance components σ^2 iteratively according to [3].

Solution of common parameters
The common parameters, are those which need to be solved using the full length of the series (e.g. x_{gia} and $x_{satbias}$). These can be solved by eliminating (i.e. solve implicitly) the time-variable parameters from all the monthly normal equation systems, and aggregating all of them into a single one:

$$N_{com} \begin{bmatrix} x_{gia} \\ x_{satbias} \end{bmatrix} = \mathbf{b}_{com} \tag{s12}$$

This system is then solved for the x_{gia} and $x_{satbias}$.

Solution of the monthly parameters
Using the estimated common parameters, we can update each monthly normal equation system, and subsequently remove (do not solve implicitly) the GIA and bias parameters. This two step approach, utilizes the uncorrelatedness of the different normal equation systems, and results in the same set of estimated parameters as if the entire system (all monthly and common parameters from all data) would have been solved in a single step[1].

Fingerprints of Ice Sheets, Glaciers and Hydrology

The Greenland and Antarctica ice sheets are discretized in 16 and 27 drainage basins (see Fig. S1), as described in [4, 5]. Over the ocean, we compute the response of the geoid to a uniform layer of 1Gt in the basin, augmenting it by a uniform shift to ensure mass conservation. The procedure, generally known as 'solving the sea level equation' is performed in the spectral domain [6], and accounts for rotational feedback. The combined effect of the basin load and the ocean, covers the entire globe and is consistent in terms of gravity, surface deformation and mass. For each basin, we now obtain two independent observables: the shifted geoid (geocentric sea level) and the associated elastic crustal deformation. From those we can trivially derive other observables, such as gravitational potential changes and relative sea level. For a constant ocean function, appropriate for the period considered here, the sea level equation is linear allowing a superposition of different contributions, conserving mass and yielding a consistent gravity and deformation response.

The construction of fingerprints for the land glaciers follows the same procedure, except that the ice load of the drainage basins are replaced by 16 clusters of glaciers (see Fig. S1). Glacier positions are taken fom the WGI/GLIMS database [7], and are grouped per region.

Another important mass signal originates from terrestrial variations in hydrology. We have analyzed monthly grids of total water storages from the WaterGap Global Hydrology Model (WGHM)[8], and took the first 60 leading EOF's as fingerprints. These modes explain more than 99% of the model variance, and are therefore adequate to capture a wide range of different hydrological signals. In the EOF analysis we discarded cells which were in glacier regions, and on Greenland. Again, a consistent passive sea level response over the ocean was computed for each mode with the procedure above.

Glacial Isostatic Adjustment
Modelling the gravity and sea level signals of glacial isostatic adjustment has been recognized as a major source of error in closing the sea level budget [9]. Therefore, we have chosen to represent the GIA signal by 5 complementary patterns, and adjust these within the inversion. To parameterize the GIA signal, we used modelling results from [10], who used a visco-elastic Earth model (VM2), and forced it with the ice loading history ICE-5G [11], augmented with a loading history in Greenland. Besides this reference run, different runs were produced in which the ocean coastline remained fixed but 5 different melting sources (Laurentide, Fennoscandia, Antarctica, Greenland, and the

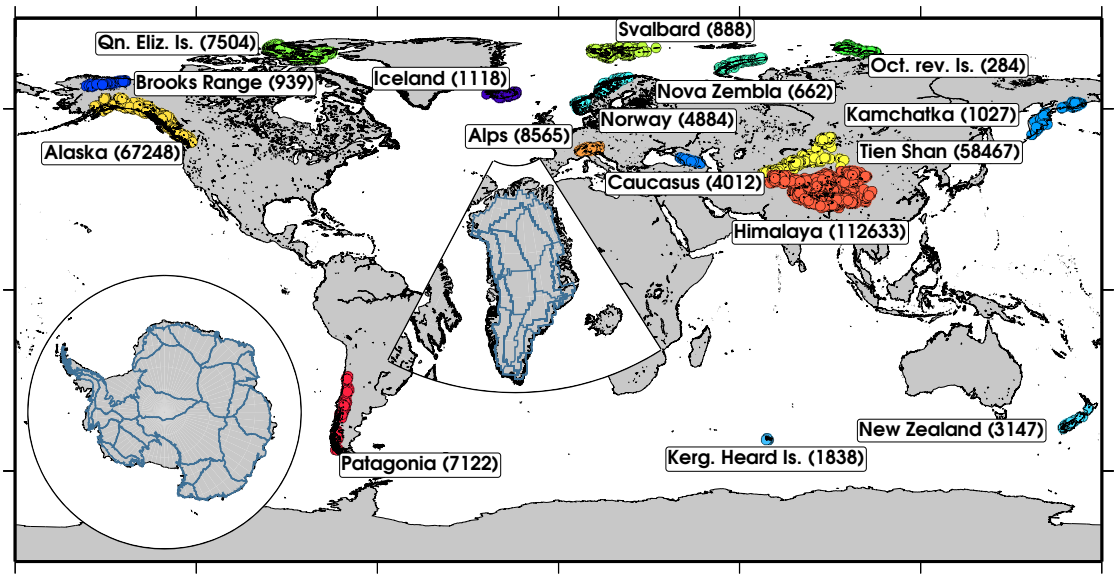

Figure S1: Overview of the used glacier clusters (numbers in between brackets are the amount of point loads per cluster) and ice sheet delineation

remainder of the load) were allowed to vary. For present day rates, the 5 different contributions approximately add up to the reference run, and can therefore be used to parameterize the GIA signal. A priori, we correct the GRACE and altimetry data with the reference run. In the inversion step, we subsequently estimate 5 different source corrections to the reference model, in order to absorb GIA-model deficiencies. The estimation of the GIA parameters is ill-posed and requires a stabilization (see the paragraph on stabilization below). The estimated GIA parameters and their effect on global mean sea level are tabulated in table S1 and S2.

Steric and Auxiliary Fingerprints

Steric changes in the ocean were computed by integrating salinity and temperature induced volume changes from the Finite Element Sea Ice Model (FESOM). The first 200 EOFs, accounting for more then 99% of the modelled steric height variances, were then used to parameterize the steric changes.

After an initial inversion, it turned out that still significant large scale non-stochastic signal exists in the altimetry residuals (see Fig. S2). For this reason, a second set of patterns have been constructed. These have been computed as follows: after the initial inversion, the altimetric height residuals have been gridded and consequently smoothed by a 200km Gaussian filter (the high resolution signal is not of interest here). An additional EOF analysis has been applied to these smoothed grids and the first 100 EOFs (explaining more than 97% of the smoothed residuals) are now used as additional fingerprints in the inversion. The use of those additional fingerprints absorb a significant part of the altimetry residuals as can be seen from Fig. S2.

During the review of a previous version of this paper, concerns arose about the sensitivity of the inversion results to the chosen steric parameterization. To illustrate the effect of the chosen steric patterns, we have constructed an additional inversion, where we used patterns obtained from the steric heights computed from the gridded Ishii data (first 1500m) [12]. For this inversion we've used a dedicated set of auxiliary patterns computed from the residuals. Similar to figure 2 of the main article, the associated global and regional sea level budget is depicted in figure S3. It can be observed that the combined total trends only change within the errorbars. Interesting is to see that more signal is absorbed in the global mean steric trend when using the steric patterns derived from the FESOM model. Only 1.2±0.3 mm/yr (versus 1.4±0.16 mm/yr) of the steric trend can be explained when using the patterns from the Ishii data. On regional scales, there may be regions where the patterns from the Ishii data may perform better (for example in the Mediterranean, where the discretization of FESOM may not be sufficiently dense). However, in the current paper we decided to stick with the patterns from FESOM as it provides estimates which are entirely independent on the ARGO data and cover the full ocean column.

Furthermore, we would like to emphasize that the applied inversion scheme results in steric changes which are significantly different from that of the FESOM model itself. This is illustrated in S4, where the first 8 estimated principal components (explaining 81% of the model variance), are compared with the PC's as computed from the model. For comparison, the steric heights from the the Ishii data [12], are projected on the same EOF's and are also plotted. It can be seen that the estimated PC's from the inversion differ significantly from the

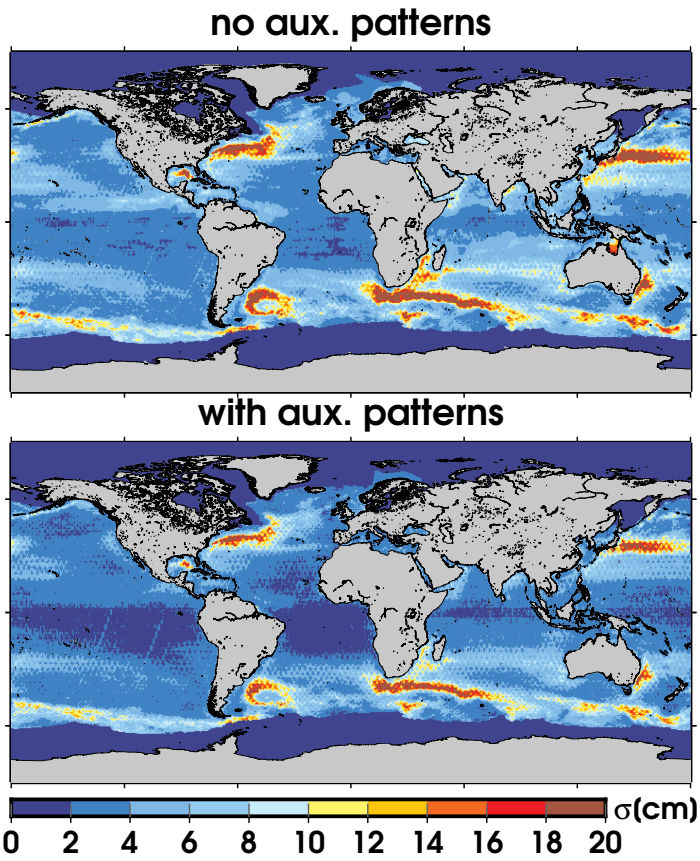

Figure S2: Standard deviation of the altimetry residuals from an inversion without auxiliary patterns (top), and residuals from an inversion using 100 auxiliary patterns(bottom).

model ones, and are in some cases even closer to the PC's from the Ishii data. In conclusion, it seems that the inversion scheme is very forgiving with regards to imperfections in the ocean model.

Stabilization of the Solution

When some patterns (i.e. columns) in matrix **B**, **C** or **D** (see equations 1 and 2 of the main paper) are very similar a (near) rank defect occurs in the normal equation systems. Two such near-rank defects play a role in the inversion. These are mitigated by adding additional constraints to the solution, as described below.

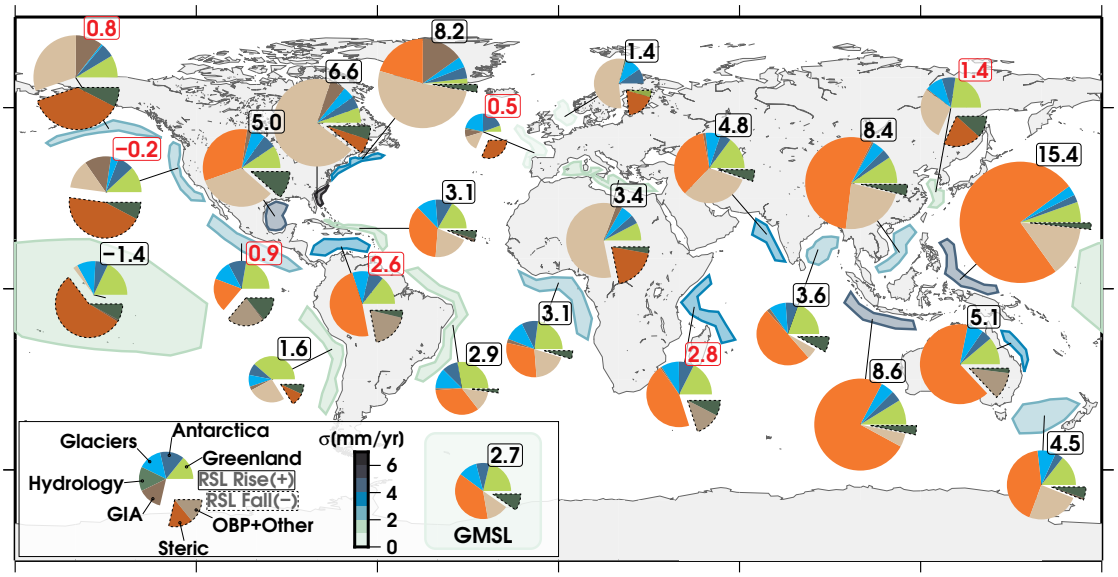

Figure S3: As in Figure 2 of the main article, but the steric fingerprints are now the first 200 leading EOFs of the steric heights from the top 1500m of the Ishii data. In addition, a new set of 100 auxiliary patterns have been computed from the smoothed altimetry residuals as well. Note that the computed total trends have changed, but only within the errorbars.

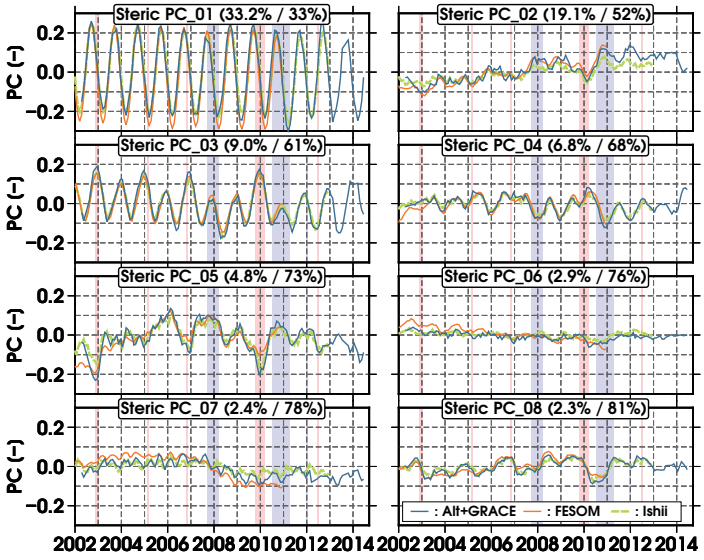

Figure S4: Estimated and computed time series of the first 8 principal components of global steric sea level. The percentages denote how much variance of the FESOM model is explained by the mode (first value indicates %per mode, second value is the cumulative percentage). The curves from the Ishii data are constructed by projecting the computed steric heights onto the modes.

The delineation of some of the basins in Greenland and Antarctica may be too fine to be resolved by the GRACE data, which can only detect signals with large spatial scales (in the order of 100's of km). Within the inversion scheme, the resolving of small basins, particular those which are elongated in north-south direction, therefore introduces strong correlations in some of the estimated ice-sheet parameters[13]. To mitigate this, a constraint has been applied, which penalizes differences between the 20 most sensitive basin combinations in Greenland and Antarctica [1].

A second near-rank defect is caused by the separation of the GIA signal from the overlying mass changes in Greenland and Antarctica. In particular, the fingerprints of the West-Antarctic drainage basins are highly correlated with the Antarctic GIA fingerprint. Recent efforts to separate the GIA signal from present day mass loss in the West Antarctic, exploit a priori information to stabilize the inversion [14]. Here, we have applied a Tikhonov constraint to the GIA parameters. In terms of the normal matrix trace, the constraint determines about 40% and the data the remaining 60% of the GIA parameters. The estimated GIA parameters and effect on sea level are tabulated in table S1 and S2. Interesting is

Table S1: Estimated GIA signal in terms of percentage of the a priori GIA model (based on VM-2 and ICE-5G). 100% means that the estimated GIA component equals the a priori GIA model. The last column describe smaller glacial masses falling outside the major glacial domes.

Laurentide	Antarctica	Fennoscandia	Greenland	other
109%	18%	63%	77%	100%

Table S2: Change in global ocean mean mass contributions (in mm/yr) due to the GIA update compared to using the a priori GIA model

Antarctica	Greenland	Glaciers	Hydrology	Total
-0.223	-0.003	-0.022	0.049	-0.197

that the GIA signal in the Antarctic represents only 18% of the a priori model. This can be partly explained by assuming relatively low upper mantle viscosities in Antarctica as discussed in [15, 16] It is also consistent with the findings from [14].

Comparison with Published Mean Sea Level Budgets

Several other studies exist which provide different estimates of the sea level budget and/or some of its components. Although the total sea level rise agrees to a large extent, the mass component of sea level differs by a fair amount among the studies. Consequently, the derived steric rates will also be affected. Besides the chosen processing methods, there are several other factors which may all contribute to some extent to the estimated mass rates[9]. These range from GIA corrections, geocenter motion corrections, to the chosen time frame. For completeness, we have tabulated some results from other studies in Table S3. Values which agree within the errorbars with our results are highlighted in bold. Although the total sea level, as measured by altimetry, agree well between the studies, there remain several large discrepancies, above the error bars, for estimates of the glaciers and ice sheets. In some cases, mass changes are subtracted from altimetry to obtain steric trends. In such studies, uncertainties in mass changes may also propagate to uncertainties in steric sea level.

Other Coastal zones

For all of the considered coastal zones, the time variation of the diffferent components have been plotted for completeness in the figures S5-S8. The trends of the components of the sea level budget (used in fig. 2 of the main paper) are tabulated for each coastal zone in table S3.

Table S3: Comparison of mean sea level rise contributions in mm/yr from other studies. Trends which agree to those from this study within the errorbars are highlighted in bold. [(a)] The hydrological component only includes modelled anthropogenic interventions and does not include climatic fluctuations (see Table 13.1 of IPCC-AR5 WG1).

	Data	Hydr.	Gr+An+Gl	Steric	Total
This Study	GRACE (GFZ), Altimetry (2002-2014)	**-0.29±0.26**	**1.37±0.09**	**1.38 ±0.16**	**2.74±0.58**
Chen et al. [17]	GRACE (CSR), ARGO(2005-2011)	**-0.07±0.32**	1.73±0.28	0.6±0.27	**2.4±0.54**
IPCC AR5 WG1 [18]	various (1993-2010)	0.38±0.12[(a)]	**1.36±0.39**	**1.1±0.3**	**2.8 ±0.55**
Llovel et al.[19]	GRACE (CSR),Altimetry (2005-2013)	2.0±0.1		0.77±0.28	**2.78±0.32**
Llovel et al. [20]	GRACE (2002-2009)	**-0.22±0.05**			
Johnson et al. [21]	GRACE (2003-2012)	1.8±0.17			
Schrama et al. [9]	GRACE (CSR) (2003-2013)		**1.47±0.09**		
Jensen et al. [22]	GRACE (GFZ), Altimetry (2002-2009)	**-0.2±-0.04**			
Jacob et al.[23]	GRACE (CSR),(2003-2010)		**1.48±0.26**		
Riva et al. [24]	GRACE (DMT) (2003-2009)	**-0.1±0.3**	**1.1±0.2**		
Cazenave et al. [25]	GRACE, Altimetry, ARGO, modelling, etc (2003-2007)	**-0.2±0.1**	1.0±0.2	0.25±0.8	**2.5±0.4**
Dieng et al. [26]	Various T/S data and GRACE (2003-2012)	1.7±0.1		0.56±0.14	**2.82±0.1**

Table S4: Trend of the sea level budget components in mm/yr for the coastal zones considered. Errors are based upon autoregressive models of order 1 which are fitted to the post fit residuals. An exception is the GIA component, which indicate a worst-case scenario error (see the Methods and Materials of the main paper). Gray and black bold values indicate trends which are significant at the 1-σ and 2-σ level respectively.

	Total	Green.	Ant.	Glac.	Hydr.	Steric	OBP+Other	GIA
Africa(East)	2.4 (± 4.16)	**0.8 (± 0.02)**	**0.4 (± 0.06)**	**0.4 (± 0.07)**	**-0.3 (± 0.23)**	0.6 (± 1.90)	0.6 (± 0.91)	0.0 (± 0.16)
Africa(West)	**3.2 (± 2.05)**	**0.8 (± 0.02)**	**0.3 (± 0.06)**	**0.4 (± 0.07)**	-0.1 (± 0.25)	**1.9 (± 1.65)**	-0.1 (± 1.72)	0.1 (± 0.17)
Arabian Sea	**4.6 (± 2.39)**	**0.8 (± 0.02)**	**0.3 (± 0.05)**	**0.4 (± 0.06)**	**-0.3 (± 0.25)**	**4.4 (± 1.69)**	-1.0 (± 2.68)	0.1 (± 0.19)
Australia(East)	**4.8 (± 3.58)**	**0.8 (± 0.02)**	**0.3 (± 0.05)**	**0.4 (± 0.07)**	-0.1 (± 0.27)	**4.8 (± 3.03)**	-1.4 (± 2.71)	0.0 (± 0.20)
Bengal Bay	**3.8 (± 3.26)**	**0.8 (± 0.02)**	**0.3 (± 0.05)**	**0.4 (± 0.07)**	**-0.3 (± 0.27)**	1.5 (± 3.93)	**1.1 (± 0.67)**	0.1 (± 0.22)
Caribbean(East)	**3.5 (± 3.22)**	**0.6 (± 0.02)**	**0.3 (± 0.06)**	**0.4 (± 0.07)**	-0.2 (± 0.18)	0.7 (± 1.63)	1.7 (± 2.74)	-0.1 (± 0.21)
Caribbean Sea	2.0 (± 3.14)	**0.7 (± 0.02)**	**0.3 (± 0.06)**	**0.4 (± 0.07)**	-0.2 (± 0.24)	0.8 (± 2.28)	-0.0 (± 3.54)	-0.0 (± 0.24)
Central America	1.0 (± 2.03)	**0.8 (± 0.02)**	**0.4 (± 0.06)**	**0.4 (± 0.07)**	**-0.5 (± 0.26)**	-0.9 (± 2.20)	0.9 (± 1.85)	-0.0 (± 0.18)
Central Pacific	-1.4 (± 1.42)	**0.9 (± 0.02)**	**0.3 (± 0.06)**	**0.4 (± 0.07)**	**-0.4 (± 0.30)**	**-2.8 (± 1.53)**	0.2 (± 0.52)	-0.0 (± 0.10)
East China Sea	1.3 (± 1.39)	**0.9 (± 0.02)**	**0.3 (± 0.05)**	**0.4 (± 0.06)**	**-0.4 (± 0.27)**	0.0 (± 0.78)	0.2 (± 1.68)	0.0 (± 0.22)
Europe(Atlantic)	**1.0 (± 0.64)**	**0.1 (± 0.01)**	**0.3 (± 0.05)**	**0.3 (± 0.06)**	0.0 (± 0.24)	-0.5 (± 1.27)	**0.7 (± 0.66)**	0.1 (± 0.25)
Gulf of Mexico	**5.9 (± 4.40)**	**0.6 (± 0.02)**	**0.4 (± 0.07)**	**0.4 (± 0.07)**	**-0.7 (± 0.27)**	**2.2 (± 2.01)**	2.9 (± 4.41)	0.1 (± 0.22)
Indonesia	**8.3 (± 4.69)**	**0.8 (± 0.02)**	**0.3 (± 0.06)**	**0.4 (± 0.07)**	**-0.3 (± 0.27)**	**6.4 (± 3.18)**	0.5 (± 0.94)	-0.0 (± 0.21)
Mediterranean	**3.6 (± 1.83)**	**0.5 (± 0.01)**	**0.2 (± 0.05)**	**0.3 (± 0.06)**	-0.2 (± 0.21)	0.6 (± 1.69)	2.0 (± 3.99)	0.2 (± 0.24)
North Sea	**1.4 (± 1.37)**	**-0.1 (± 0.01)**	**0.3 (± 0.05)**	**0.3 (± 0.06)**	0.0 (± 0.24)	-0.3 (± 0.50)	**1.2 (± 0.97)**	0.0 (± 0.36)
Pacific(North)	0.6 (± 4.31)	**0.7 (± 0.02)**	**0.4 (± 0.08)**	0.1 (± 0.08)	**-0.6 (± 0.26)**	**-2.3 (± 1.38)**	**1.6 (± 0.63)**	**0.8 (± 0.28)**
Philippines	**14.7 (± 4.39)**	**0.9 (± 0.02)**	**0.3 (± 0.06)**	**0.4 (± 0.07)**	-0.3 (± 0.26)	**11.2 (± 3.58)**	2.2 (± 2.48)	-0.0 (± 0.17)
South China Sea	**7.6 (± 3.17)**	**0.9 (± 0.02)**	**0.3 (± 0.05)**	**0.4 (± 0.07)**	**-0.3 (± 0.27)**	**5.8 (± 2.41)**	0.5 (± 1.04)	0.1 (± 0.17)
SthAmerica(East)	**3.1 (± 1.57)**	**0.8 (± 0.02)**	**0.3 (± 0.05)**	**0.4 (± 0.07)**	-0.1 (± 0.28)	**1.6 (± 0.98)**	0.1 (± 1.73)	0.0 (± 0.09)
SthAmerica(West)	**1.7 (± 1.56)**	**0.9 (± 0.02)**	**0.2 (± 0.04)**	**0.2 (± 0.06)**	-0.1 (± 0.24)	-1.1 (± 1.62)	**1.6 (± 0.35)**	0.1 (± 0.10)
Tasman Sea	**3.8 (± 0.86)**	**0.7 (± 0.02)**	**0.2 (± 0.04)**	**0.4 (± 0.08)**	-0.3 (± 0.29)	**1.6 (± 1.33)**	**1.1 (± 0.89)**	-0.0 (± 0.23)
US(East)	**6.7 (± 3.85)**	**0.5 (± 0.01)**	**0.4 (± 0.07)**	**0.4 (± 0.07)**	**-0.4 (± 0.29)**	1.8 (± 2.11)	**3.6 (± 2.57)**	**0.5 (± 0.25)**
US(NorthEast)	**9.1 (± 1.72)**	**0.2 (± 0.01)**	**0.4 (± 0.06)**	**0.3 (± 0.07)**	**-0.2 (± 0.22)**	**1.8 (± 1.60)**	**5.3 (± 2.62)**	**1.3 (± 0.25)**
US(West)	-0.3 (± 2.52)	**0.7 (± 0.02)**	**0.4 (± 0.08)**	**0.2 (± 0.07)**	**-0.4 (± 0.24)**	**-2.0 (± 1.49)**	0.2 (± 2.15)	**0.7 (± 0.16)**

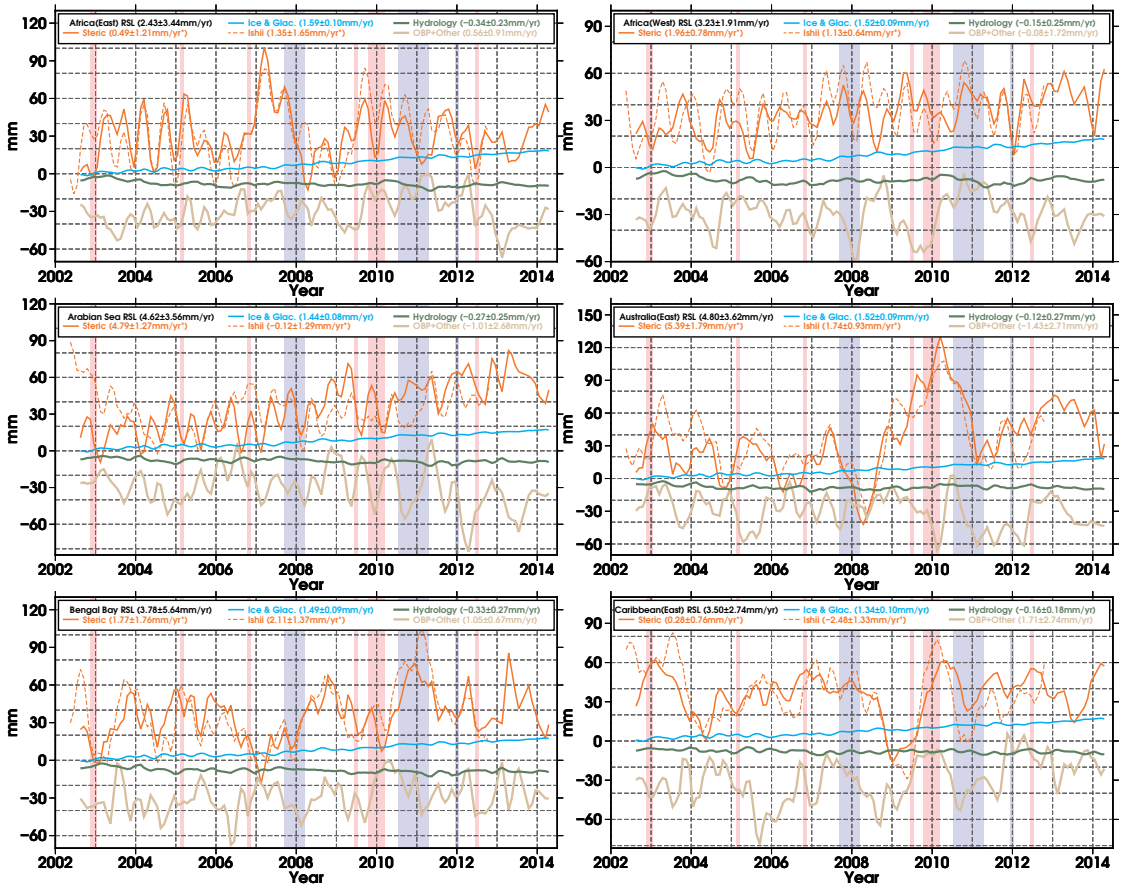

Figure S5: Time variable sea level contributions for varying coastal regions. Warm (El Niño, red) and cold (La Niña, blue) phases are highlighted, whenever the Multivariate ENSO Index (MEI) gets larger than 1 or smaller than -1 respectively. Trends with an asterisk indicate that they are computed over the period where Ishii data is available (2002-2012).

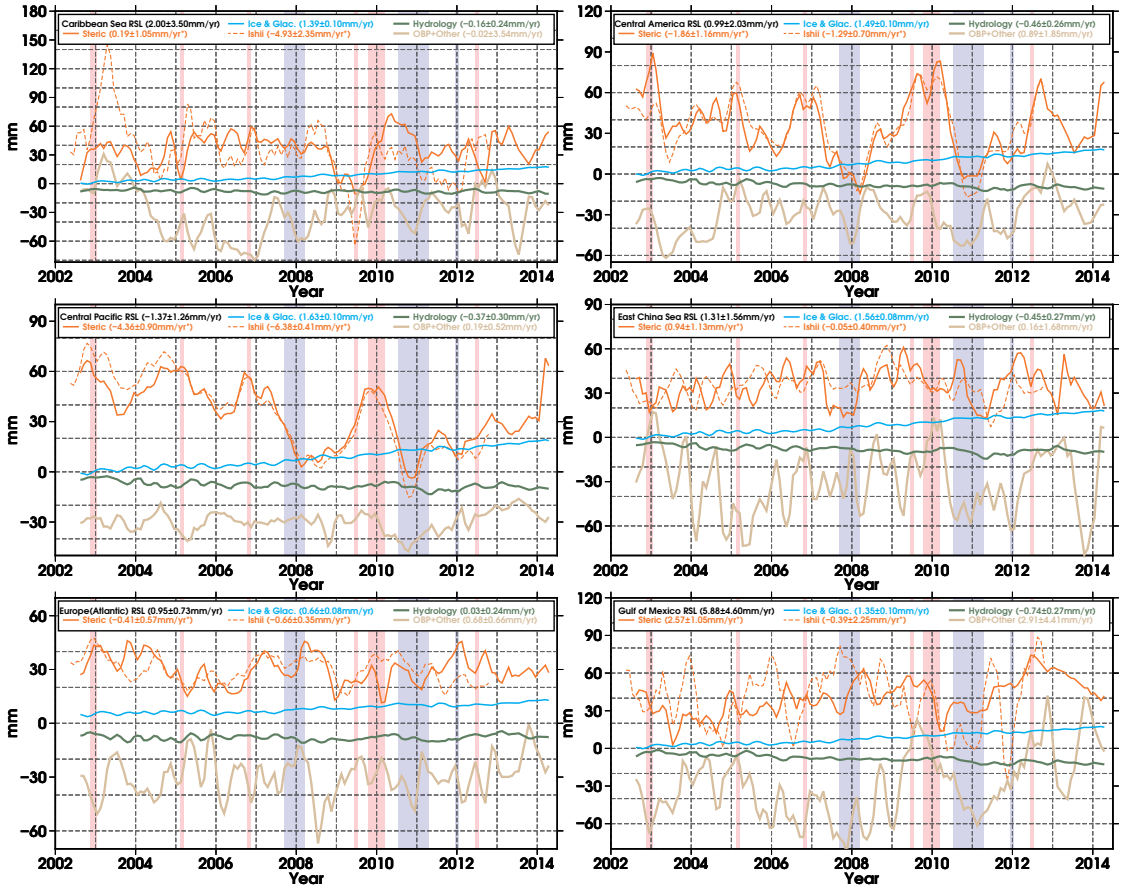

Figure S6: As in Fig. S5 but for various additional regions

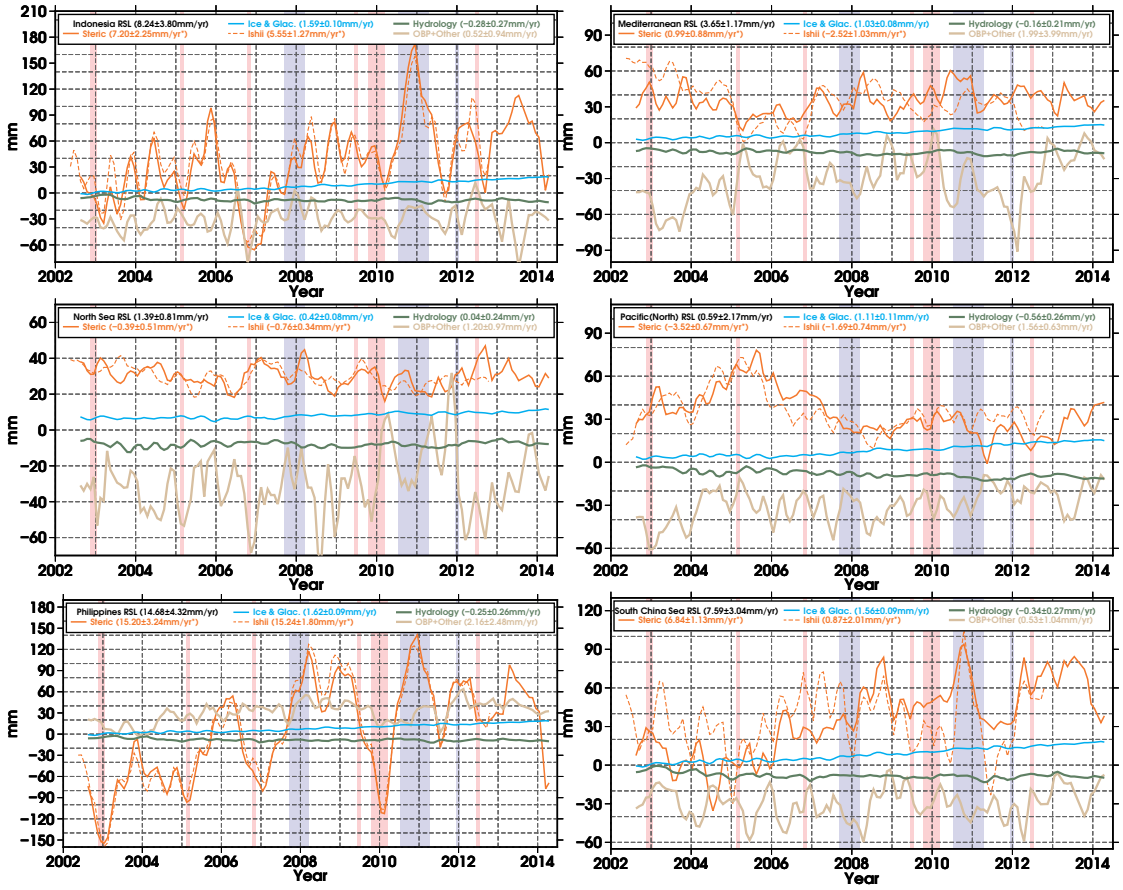

Figure S7: As in Fig. S5 but for various additional regions

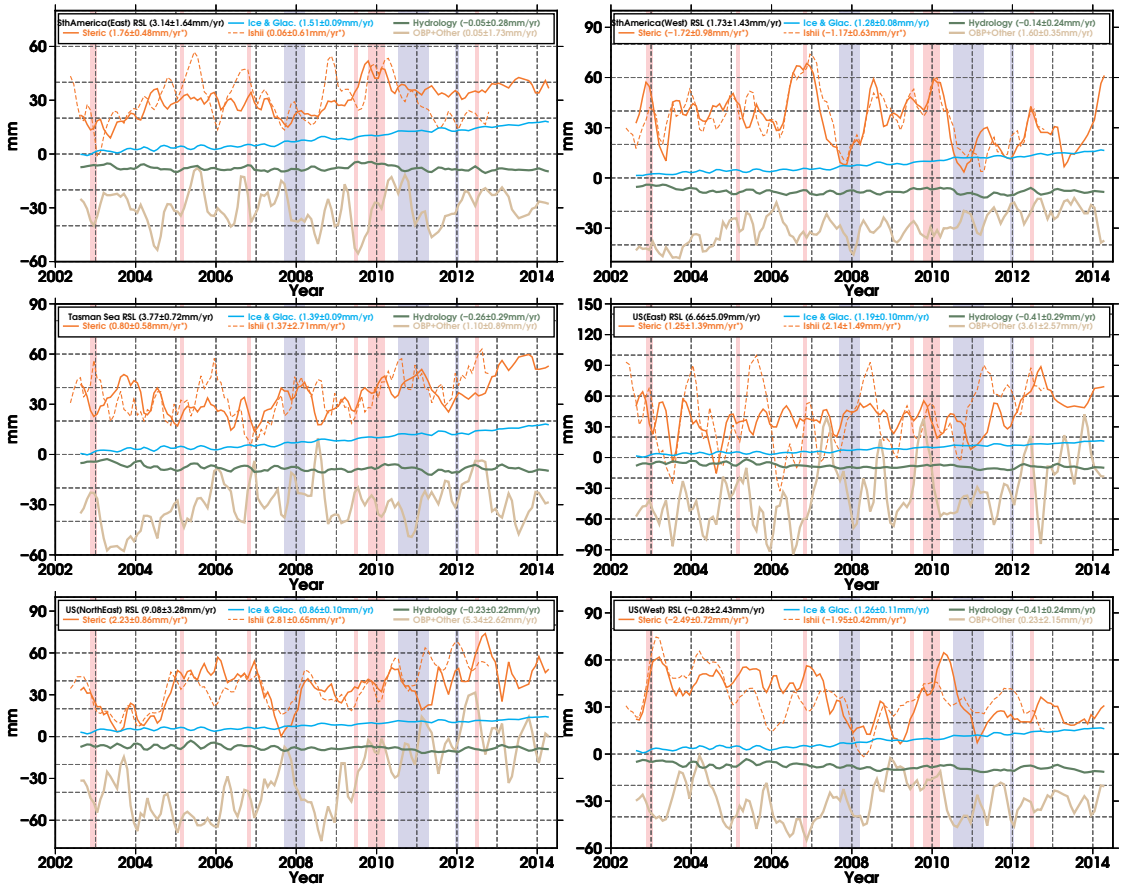

Figure S8: As in Fig. S5 but for various additional regions

References

[1] Rietbroek, R. (2014) Ph.D. thesis (Institute of Geodesy and Geoinformation, Faculty of Agriculture, University of Bonn).

[2] Koch, K.-R. (1988) *Parameter estimation and hypothesis testing in linear models*. (Springer-Verlag New York, Inc.).

[3] Förstner, W. (1979) Ein verfahren zur schätzung von varianz-und kovarianzkomponenten. *Allgemeine Vermessungsnachrichten* **86**, 446–453.

[4] Wouters, B, Chambers, D, & Schrama, E. J. O. (2008) Grace observes small-scale mass loss in greenland. *Geophysical Research Letters* **35**, L20501.

[5] Zwally, H & Giovinetto, M. (2011) Overview and assessment of antarctic ice-sheet mass balance estimates: 1992–2009. *Surveys in Geophysics* **32**, 351–376.

[6] Dahlen, F. A. (1976) The passive influence of the oceans upon the rotation of the earth. *Geophysical Journal of the Royal Astronomical Society* **46**, 363–406.

[7] Raup, B, Racoviteanu, A, Khalsa, S, Helm, C, R, A, & Arnaud, Y. (2007) The glims geospatial glacier database: A new tool for studying glacier change. *Global and Planetary Change* **56**, 101.

[8] Döll, P, Kaspar, F, & Lehner, B. (2003) A global hydrological model for deriving water availability indicators: model tuning and validation. *Journal of Hydrology* **270**, 105–134.

[9] Schrama, E, Wouters, B, & Rietbroek, R. (2014) A mascon approach to assess ice sheet and glacier mass balances and their uncertainties from grace data. *Journal of Geophysical Research: Solid Earth* **119**, 6048âĂŞ6066.

[10] Klemann, V & Martinec, Z. (2011) Contribution of glacial-isostatic adjustment to the geocenter motion. *Tectonophysics* **511**, 99–108.

[11] Peltier, W. (2004) Global glacial isostasy and the surface of the ice-age earth: The ice-5g (vm2) model and grace. *Annual Review of Earth and Planetary Sciences* **32**, 111.

[12] Ishii, M & Kimoto, M. (2009) Reevaluation of historical ocean heat content variations with time-varying xbt and mbt depth bias corrections. *Journal of Oceanography* **65**, 287–299.

[13] Rietbroek, R, Brunnabend, S. E, Kusche, J, & Schröter, J. (2012) Resolving sea level contributions by identifying fingerprints in time-variable gravity and altimetry. *Journal of Geodynamics* **59**, 72–81.

[14] Schoen, N, Zammit-Mangion, A, Rougier, J. C, Flament, T, Rémy, F, Luthcke, S, & Bamber, J. L. (2015) Simultaneous solution for mass trends on the west antarctic ice sheet. *The Cryosphere* **9**, 805–819.

[15] Sasgen, I, Konrad, H, Ivins, E, Van den Broeke, M, Bamber, J, Martinec, Z, Klemann, V, et al. (2013) Antarctic ice-mass balance 2003 to 2012: regional reanalysis of grace satellite gravimetry measurements with improved estimate of glacial-isostatic adjustment based on gps uplift rates. *The Cryosphere* **7**, 1499–1512.

[16] Whitehouse, P. L, Bentley, M. J, Milne, G. A, King, M. A, & Thomas, I. D. (2012) A new glacial isostatic adjustment model for antarctica: calibrated and tested using observations of relative sea-level change and present-day uplift rates. *Geophysical Journal International* **190**, 1464–1482.

[17] Chen, J, Wilson, C, & Tapley, B. (2013) Contribution of ice sheet and mountain glacier melt to recent sea level rise. *Nature Geoscience* **6**, 549–552.

[18] Stocker, T. F, Qin, D, Plattner, G.-K, Tignor, M, Allen, S. K, Boschung, J, Nauels, A, Xia, Y, Bex, V, & Midgley, P. M. (2013) Climate change 2013: The physical science basis. *Intergovernmental Panel on Climate Change, Working Group I Contribution to the IPCC Fifth Assessment Report (AR5)(Cambridge Univ Press, New York)*.

[19] Llovel, W, Willis, J, Landerer, F, & Fukumori, I. (2014) Deep-ocean contribution to sea level and energy budget not detectable over the past decade. *Nature Climate Change*.

[20] Llovel, W, Becker, M, Cazenave, A, Crétaux, J.-F, & Ramillien, G. (2010) Global land water storage change from grace over 2002–2009; inference on sea level. *Comptes Rendus Geosciences* **342**, 179–188.

[21] Johnson, G. C & Chambers, D. P. (2013) Ocean bottom pressure seasonal cycles and decadal trends from grace release-05: Ocean circulation implications. *Journal of Geophysical Research: Oceans* **118**, 4228–4240.

[22] Jensen, L, Rietbroek, R, & Kusche, J. (2013) Land water contribution to sea level from grace and jason-1measurements. *Journal of Geophysical Research: Oceans* **118**, 212–226.

[23] Jacob, T, Wahr, J, Pfeffer, W, & Swenson, S. (2012) Recent contributions of glaciers and ice caps to sea level rise. *Nature*.

[24] Riva, R. E. M, Bamber, J. L, Lavallée, D. A, & Wouters, B. (2010) Sea-level fingerprint of continental water and ice mass change from grace. *Geophysical Research Letters* **37**, L19605.

[25] Cazenave, A & Llovel, W. (2010) Contemporary sea level rise. *Annual Review of Marine Science* **2**, 145–173.

[26] Dieng, H. B, Palanisamy, H, Cazenave, A, Meyssignac, B, & von Schuckmann, K. (2015) The sea level budget since 2003: Inference on the deep ocean heat content. *Surveys in Geophysics* **36**, 209–229.